International Journal of Engineering Trends and Technology
ISSN: 2231–5381 / https://doi.org/10.14445/22315381/IJETT-V73I1P117

Volume 73 Issue 1, 192-206, January 2025

Original Article

Development of a Thermoacoustically-Driven Thermoacoustic Refrigerator Powered by Residual Heat

Pacifique Mugisho[1], Lagouge Tartibu[2]

[1]*Mechanical Engineering, Mapon University, Kindu, Democratic Republic of Congo.*
[2]*Mechanical and Industrial Engineering Technology, University of Johannesburg, Johannesburg, South Africa.*

[1]*Corresponding Author: pacymugisho@gmail.com*

Received: 23 September 2024 Revised: 09 November 2024 Accepted: 07 December 2024 Published: 31 January 2025

Abstract - *This article presents the design and analysis of a Thermoacoustically-Driven Thermoacoustic Refrigerator (TADTAR) powered by waste heat. The primary objective is to develop an efficient refrigeration system that offers significant cooling capacity while minimizing energy consumption and emissions associated with conventional refrigeration methods. By leveraging the thermoacoustic effect, the TADTAR converts waste heat into acoustic energy, which is then used to transfer heat from a cold source to a hot source. Advanced modeling and simulation techniques using DeltaEC software were employed to analyse key parameters influencing the system's performance. The suitable TADTAR configuration achieved a maximum Coefficient of Performance (COP) of 4 and an overall efficiency of 73.09% of the Carnot efficiency, demonstrating its competitive potential compared to traditional refrigeration technologies. Material selection and design parameters were found to be crucial in enhancing system performance. The research suggests broader applications for the TADTAR system across various sectors, including industrial processes and transportation. Further experimental validation is advocated to confirm the practicality and reliability of the TADTAR system in real-world applications, supporting the transition to more sustainable refrigeration solutions.*

Keywords - *Thermoacoustic, Refrigeration, Cooling, TADTAR, Waste heat, Soundwave, Acoustic.*

1. Introduction

The world grapples with pressing climate challenges, including greenhouse gas emissions and ozone depletion, exacerbated by automobile engine waste and the widespread use of Hydrofluorocarbons (HFCs) and Chlorofluorocarbons (CFCs) in refrigeration and air conditioning systems [1,2]. Heavy vehicles significantly contribute to this crisis, emitting greenhouse gases equivalent to approximately 60 light vehicles. Their emissions constitute around 25% of the European Union's total and a quarter of road transport emissions [3]. Addressing these issues demands innovative engine and refrigeration technologies. Extensive research focuses on recovering exhaust gas waste heat, which accounts for nearly 60% of total engine energy, with only 40% currently utilized and 15% recovered by turbochargers. The remaining 45% is wasted [. Simultaneously, significant strides are being made in phasing out harmful refrigerants like CFCs and HFCs in favor of more sustainable alternatives, including hydrofluoro-olefins (HFOs), which have low global warming potential, and natural refrigerants like ammonia and CO_2 [4]. Thermoacoustics presents a promising solution for waste heat utilization by harnessing the interaction between heat and sound. This technology converts thermal energy into acoustic energy through Thermoacoustic Engines (TAEs) or, conversely, converts acoustic energy back into cooling through Thermoacoustic Refrigerators (TARs) [5]. As illustrated in Figure 1, a thermoacoustic system typically consists of an acoustic resonator, an acoustic source, and an inert gas. The core component is a porous medium known as a "stack" in standing wave configuration or "regenerator" in traveling wave configuration, positioned between two Heat Exchangers (HX). In TAEs, heat is converted into power, while TARs consume power to transfer heat from a cold to a hot source.

As depicted in Figure 2, in the engine configuration, heat (Q_H) is transferred from the hot source (T_H) to the cold sink (T_0), generating power (W). Conversely, in the refrigerator configuration, input power (W) extracts heat (Q_C) from the cold source (T_C) and rejects it to the hot sink (T_0) as heat (Q_0). Thermoacoustic technologies are renowned for their simplicity and low maintenance requirements. They efficiently harness low-grade heat sources, such as industrial waste, solar energy, or combustion gases. The prevalence of waste heat in vehicles makes them prime candidates for thermoacoustic refrigeration systems [2, 6]. Building on previous technologies, a combined system replaces the TAR's sound source with the acoustic wave generated by a TAE.

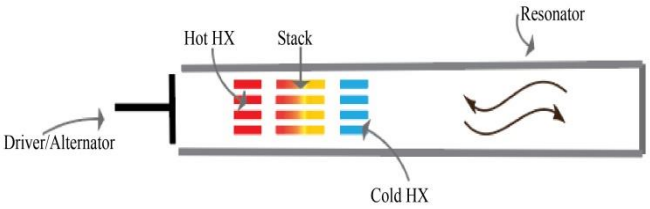

Fig. 1 Schematic of a thermoacoustic refrigerator

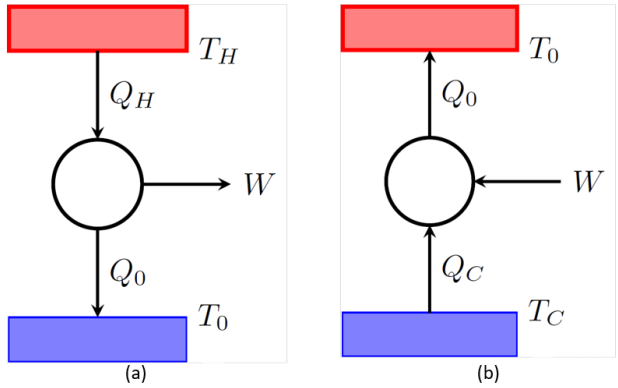

Fig. 2 Schematic representation of an engine (a) and refrigerator (b) configurations.

This integrated system is termed a Thermoacoustically-Driven Thermoacoustic Refrigerator (TADTAR). When powered by heat, it becomes a Heat Driven Thermoacoustic Refrigerator (HDTAR) [2]. Heat input can originate from various renewable sources, including electricity, solar energy, or waste heat. Figure 3 depicts a combined model where heat is supplied to the TAE's Hot Heat Exchanger (HHX) and extracted from the TAR's Cold Heat Exchanger (CHX), with the Ambient Heat Exchangers (AHXs) serving as heat sinks. To address growing environmental concerns, this study proposes a refrigeration and air conditioning system utilizing a noble gas refrigerant. Capitalizing on the substantial thermal energy loss (approximately 60%) from thermal engines, the system employs exhaust gas heat to power a thermoacoustic engine, driving a thermoacoustic refrigerator for cabin cooling. The primary goal is to develop a thermoacoustic refrigerator that delivers sufficient cooling capacity for heavy vehicles. Key parameters influencing the coefficient of performance (COP) and overall efficiency will be improved for optimal heavy-duty vehicle integration.

2. Related Works

Thermoacoustic systems are primarily categorized into standing wave and traveling wave configurations. In a standing wave system, the sound wave is confined within the resonator, forming stationary patterns of pressure and velocity nodes and antinodes. Typically positioned at a velocity antinode, the stackacilitates heat transfer to drive the acoustic wave [7, 8]. Conversely, a traveling wave system employs a continuously propagating sound wave within a closed-loop resonator. The regenerator, placed in the wave path, enables efficient heat exchange [9, 10].

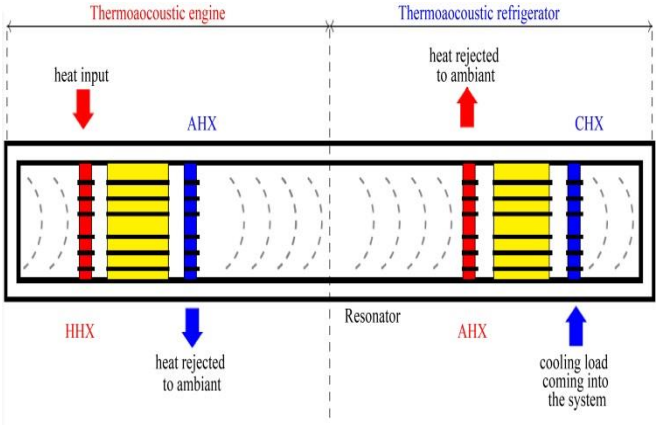

Fig. 3 Representation of a thermoacoustically-driven thermoacoustic

Several studies have significantly advanced thermoacoustic refrigeration. Duffourd [11] investigated a miniature TAR, examining the influence of plate geometry, stack location, and standing wave amplitude on the temperature differential. Dhuley and Altrey [12], following Tijani et al.'s guidelines [13], designed a TAE achieving a $4\,W$ cooling power at $210\,K$ using helium. Syeda developed a speaker-driven TAR reaching $-67℃$ with a $4\,W$ cooling power and $75\,K$ temperature difference. Optimizing stack placement and using helium noble gas mixtures enhanced performance by reducing the Prandtl number. Additionally, Kamil et al. [1] optimized a standing wave TAR using DeltaEC, targeting a $25℃$ temperature difference with helium. They analysed stack and resonator parameters, selecting Mylar for its superior thermal properties. Prashantha et al. [14] designed a helium-based thermoacoustic loudspeaker refrigerator, achieving a $50\,W$ cooling power and $75\,K$ temperature difference at 10 bar. DeltaEC predicted cold heat exchanger temperatures of $-3.4℃$ and $-4.3℃$ for third and quarter wavelength resonators, respectively.

These studies collectively demonstrate significant advancements in thermoacoustic refrigeration, emphasizing the importance of material selection, geometric configuration, and precise parameter control for efficient cooling. Thermoacoustic technology presents a promising concept for converting solar heat directly into cooling. Currently, it is the only device capable of handling such high-temperature levels, allowing greater efficiency compared to adsorption or absorption systems. For example, Adeff and Hoffler [6] designed a solar-powered thermoacoustic refrigerator producing a cooling power of $2.5\,W$ at a cold temperature of $5℃$. Using a $0.457\,m$ diameter Fresnel lens, sunlight was concentrated directly onto a stack made of cross-linked glassy carbon, heating it to $475℃$ and thus eliminating the need for a hot heat exchanger. However, the solar receiver design could be improved by focusing sunlight on a heat exchanger instead of directly on the stack, reducing heat dissipation. Cordillet [15] proposed an appropriate thermal design for this configuration, achieving $1\,kW$ of cooling capacity at $-25℃$

through developed simulation tools and experimental equipment. Similar models are discussed by Tijani et al. [7], who constructed a TADTAR producing $-20℃$. Thermoacoustic technology also has significant advantages in waste heat recovery across various industries, including process, construction, and transportation. For example, it can convert $100\,kW$ of residual heat at $160℃$ into $100\,kW$ of electricity via a thermoacoustic energy generator or couple a waste heat-powered engine with a heat pump to manage heat levels. In the automotive sector, thermoacoustic technology can be applied in multiple ways. Zoontjens et al. [2] conducted a feasibility study on HDTAR for vehicle interior cooling, potentially replacing vapor compression systems. Their study found that an Automotive Thermoacoustic Refrigerator (ATAR) could utilize exhaust gas heat to pump heat into the vehicle's passenger compartment via a thermoacoustic heat pump. This system is cost-effective, has low maintenance costs, and uses environmentally friendly gases (such as air, argon, and helium). However, its effectiveness is limited to 40% of the Carnot coefficient due to thermal losses and viscous dissipation, though performance can be improved with optimal stack parameters and resonator geometry.

Previous research designed and built a standing wave TADTAR operating at $600℃$ with a heating power of $1000\,W$. They used a honeycomb ceramic stack resistant to $1600℃$ and found that maximum efficiency is achieved when the TAE stack is approximately $\lambda/20$ from the pressure anti-node (where λ represents the wavelength). Spoelstra [16] studied a traveling wave thermoacoustic refrigerator driven by a thermoacoustic engine at a maximum helium pressure of $38\,bar$ and an operating frequency of $123\,Hz$, achieving a maximum Carnot performance of 33%. Saechan and Dhuchakallaya [17] investigated a TADTAR in a loop tube configuration operating at $58.6\,Hz$, producing a cooling temperature of $-3.6℃$.

Their experimental results indicated sufficient cooling power for medicine storage in rural areas, aligning with the SCORE project objectives. Farikhah [18] further studied this configuration, optimizing parameters such as the relative position between the stack, the radius of the engine stack and refrigerator, and the porosity of both stacks, finding optimal stack radii of $0.70\,mm$ for the engine and $0.078\,mm$ for the refrigerator. Bouramdane et al. [19] examined the impact of plate configuration in TADTAR systems, concluding that while spiral plate stacking is most suitable for the thermoacoustic engine, flat plates generate a higher temperature difference in the thermoacoustic refrigerator. Desai et al. [20] conducted an experimental study on a TADTAR operating in a standing wave configuration. Their research aimed to enhance the TADTAR's performance by exploring different working gases and adjusting key geometric parameters, namely the resonator length and TAR stack position. By keeping the TAE configuration constant and varying the TAR geometry, they identified a specific stack length and position that maximized the TADTAR's performance. This optimal configuration resulted in a significant pressure amplitude of $82.96\,K$ and a substantial temperature difference of $16.3\,K$ across the TAR stack. Existing literature has explored the relationship between the geometric parameters of thermoacoustic systems and their performance. While research on TARs is relatively abundant, studies on TADTARs, which combine thermoacoustic engines and refrigerators, are less common. Moreover, existing TADTAR research often lacks a comprehensive analysis considering the geometric configurations of both the TAE and TAR components. To address this gap, this study focuses on developing a TADTAR and analyzing its performance based on key geometric parameters: stack position, stack length, stack spacing, and stack thickness on both the TAE and TAR sides. The paper provides a detailed analysis of the TADTAR's output, including temperature difference, pressure amplitude, frequency, and coefficient of performance generated by the system in relation to the heat input.

3. Design Methodology

Based on the concepts developed in the literature [17], two configurations were selected, notably a standing and traveling wave TADTAR, as depicted in Figures 4 and 5, respectively. The software tool DeltaEC (Design Environment for Low-amplitude Thermoacoustic Energy Conversion) was used to develop the proposed models describing the thermoacoustic systems. Both configurations share the same TAE and TAR stack and heat exchanger geometries, enabling a direct comparison of performance based on the coefficient of performance (COP). The standing wave configuration comprises a DUCT (resonator tube), HX (heat exchanger), STKSLAB (stack), CONE (resonator part), and COMPLIANCE. By positioning the stack proximate to the acoustic source, this setup induces a standing wave pattern within the resonator. Consequently, maximum pressure and acoustic velocity are attained at the resonator's antinode and node, respectively.

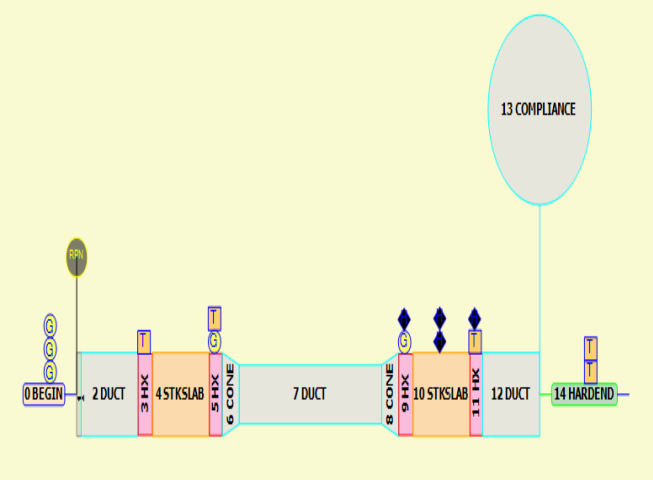

Fig. 4 Standing wave TADTAR

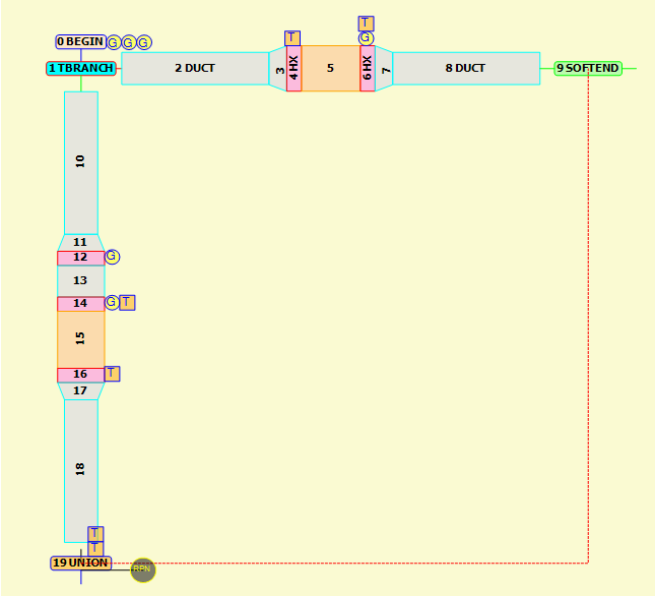

Fig. 5 Traveling wave TADTAR

The traveling wave configuration comprises a DUCT, HX, STKSLAB, and CONE. Unlike the standing wave setup, this configuration incorporates an additional ambient heat exchanger for enhanced heat management. Operating as a single-stage system with a closed-loop engine and refrigerator, this configuration shares similarities with the previous design but features a longer, 6.6 m resonator.

The resonator is divided into a 1.72 m engine section and a 1.58 m refrigerator section. Pressure amplitude and acoustic velocity are strategically positioned at nodal points to sustain a travelling wave. Geometric specifications for both the standing and traveling wave configurations are tabulated in Table 1. The proposed methodology workflow for designing the TADTAR in DeltaEC is illustrated in Figure 6. The first step involves selecting the most suitable materials (MP) for designing the system.

Afterwards, the geometrical parameters (GeoP) of the resonator, stack and heat exchangers are selected. Following this, the global parameters (GP), such as the sound-wave frequency, mean pressure, temperature, volumetric velocity, acoustic pressure and input heat at the hot heat exchanger, are defined. Some parameters are fixed, while others are variables designated as 'Target' and 'Guess' parameters in DeltaEC. DeltaEC solves differential equations for the pressure, temperature, acoustic power, and enthalpy by running the simulation and guessing the fitted solution that converges with target parameters.

Meanwhile, the geometrical, global and materials parameters that maximize acoustic power and heat energy while minimizing acoustic power loss are tracked to evaluate the Coefficient of Performance (COP), which serves as the performance index for selecting the TADTAR configuration. The Reverse Polish Notation (RPN) is used to deduce cooling power and COP in DeltaEC across a residual heat range of 2 to 10 kW.

Once the performance index is computed, the best configuration is selected to conduct the numerical analysis of the TADTAR to evaluate the system's behavior under varying parameters. Thus, the impact of geometric factors, including stack length (L_s), stack position (x_s), plate spacing ($2y_0$), plate thickness (t), and pore number (N) on overall system performance have been evaluated. Each simulation was performed by keeping other parameters fixed, and the best geometrical configurations maximizing the performance index were selected. The best TADTAR geometrical configuration was finally used to re-evaluate the overall COP of the system.

Table 1. Geometrical parameters

	Parts	Parameters	Values
Engine	Ambient HX	Length [m]	0.045
		Diameter [m]	0.16
		Porosity	0.97
		Plate spacing 10^{-4}[mm]	4.83
	Stack	Length [m]	0.2
		Diameter [m]	0.16
		Porosity	0.16
		Hydraulic radius [mm]	0.08
	Hot HX	Length [m]	0.05
		Diameter [m]	0.16
		Porosity	0.95
		Plate spacing 10^{-4}[mm]	2.243
Refrigerator	Ambient HX	Length [m]	0.045
		Diameter [m]	0.16
		Porosity	0.97
		Plate spacing 10^{-4}[mm]	4.83
	Stack	Length [m]	0.2
		Diameter [m]	0.16
		Porosity	1
		Hydraulic radius [mm]	0.08
	Hot HX	Length [m]	0.05
		Diameter [m]	0.16
		Porosity	0.97
		Plate spacing 10^{-4}[mm]	4.83
	Resonator	Length [m]	1.72
		Diameter [m]	0.16
	Compliance	Volume	0.025

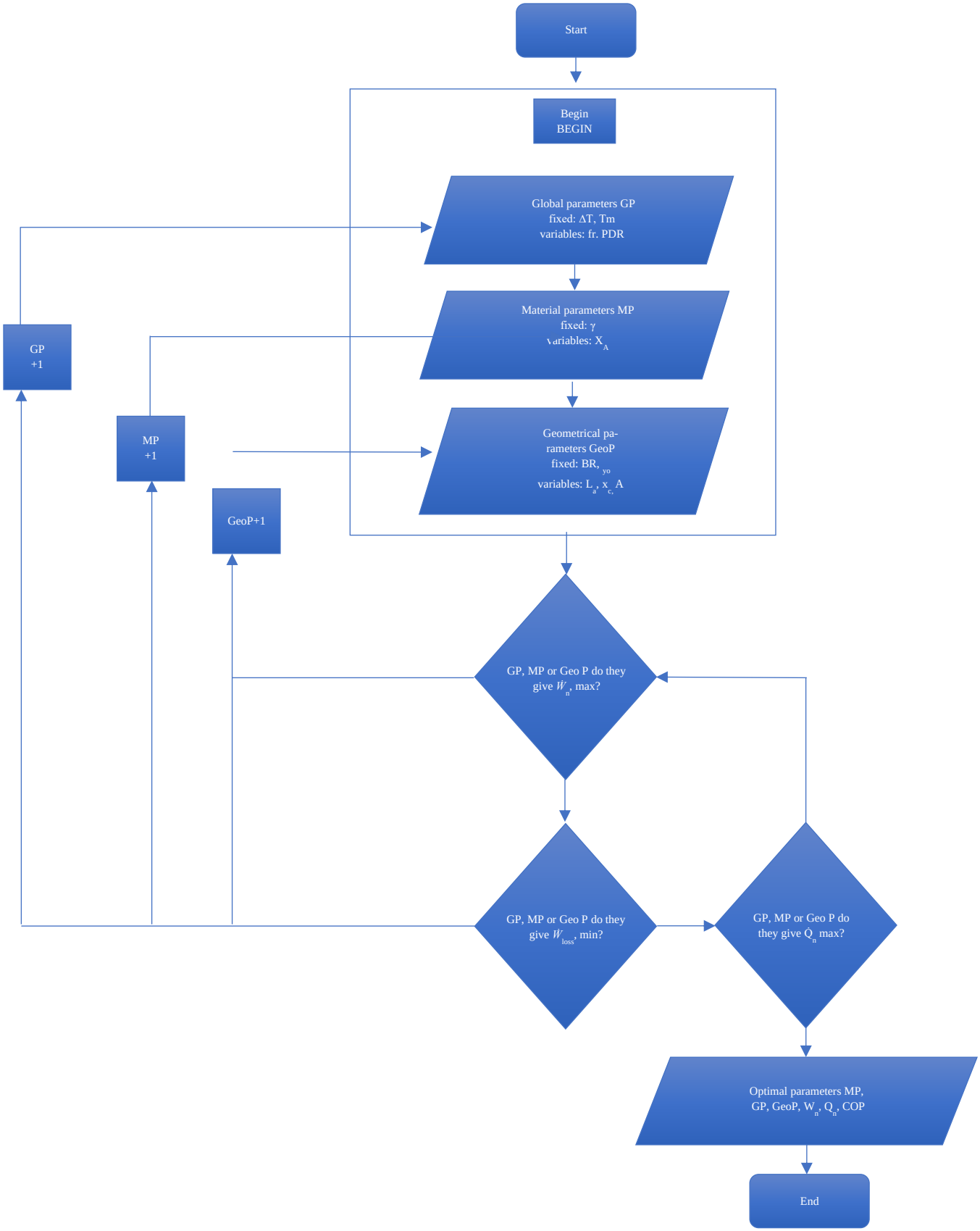

Fig. 6 Workflow of the design of the TADTAR in DeltaEC

3.1. Specifications

The primary design goal for the thermoacoustic refrigerator is to achieve a specified cooling capacity (Q_C) and cold source temperature (T_C). For this study, a Caterpillar C15 inline 6-cylinder engine, commonly used in medium to large construction and mining equipment, was selected as the heat source. Based on a typical engine's technical data sheet, the exhaust gas temperature is approximately 527℃. However, considering the cooling effect of the turbocharger, a conservative exhaust gas temperature of 400℃ was adopted. Based on specific conditions, including desired interior temperature, vehicle size, and ambient temperature, the required cooling capacity for the passenger compartment was estimated at $5372\,W$. The TADTAR in this study has the following specifications:

- **Materials**: Materials must be thermally conductive, mechanically robust and capable of withstanding temperatures up to 400℃ and high pressures.
- **Compactness**: The thermoacoustic device must fit within the available space on the vehicle while fulfilling the required cooling performance.
- **Performance**: The Coefficient of Performance (COP) of the system must be relatively high.
- **Reliability and maintenance:** The thermoacoustic device must consider factors such as durability, ease of maintenance, and the availability of spare parts.

3.2. Design Parameters

When designing a thermoacoustic system, several critical parameters must be carefully considered. These parameters, outlined in Table 2, have been extensively discussed in the literature [10]. The interdependence of these parameters makes designing more complex. Wetzel and Herman [21] proposed a method for standardizing these parameters to address this complexity. Standardized thermoacoustic parameters simplify the diverse range of existing parameters and facilitate the manipulation of system characteristics during both the design and construction phases. The standardized parameters employed in this study are presented in Table 5, allowing for an assessment of the system's COP. Therefore, the normalized working flux can be expressed as follows:

$$\begin{aligned}\dot{E}_{2n} &= \frac{\dot{E}_2}{Ap_m a} \\ &= \frac{\delta_{kn} D^2 L_{sn}(\gamma-1)B\cos^2(x_{sn})}{4\gamma} \\ &\times \left[\frac{\Delta T_{mn}\tan(x_{sn})}{BL_{sn}(\gamma-1)(1+\sqrt{\sigma})(1-\sqrt{\sigma}\,\delta_{kn}+\frac{1}{2}\sigma\delta_{kn}^2)} - 1\right] \\ &- \left[\frac{\delta_{kn} L_{sn} D^2}{4\gamma} \times \frac{\sqrt{\sigma}\sin^2(x_{sn})}{B(1-\sqrt{\sigma}\,\delta_{kn}+\frac{1}{2}\sigma\delta_{kn}^2)}\right]\end{aligned} \quad (1)$$

And the equation for the total enthalpy flow is expressed as follows:

$$\begin{aligned}\dot{H}_{2n} = \frac{\dot{H}}{Ap_m a} &= \frac{\delta_{kn} D^2 \sin(2x_{sn})}{8\gamma(1+\sigma)(1-\sqrt{\sigma}\,\delta_{kn}+\frac{1}{2}\sigma\delta_{kn}^2)} \\ &\times \left[\frac{\Delta T_{mn}\tan(x_{sn})}{(\gamma-1)BL_{sn}} \times \frac{(1+\sqrt{\sigma}+\sigma)}{1+\sqrt{\sigma}}\right. \\ &\left. - (1+\sqrt{\sigma}-\sqrt{\sigma}\,\delta_{kn})\right]\end{aligned} \quad (2)$$

Where, p_n the normalized acoustic pressure, δ_{kn} the normalized thermal penetration depth, D the drive ratio, B the blockage ratio, x_{sn} the normalized stack position, γ the compression ratio, ΔT_{mn} the normalized mean temperature and σ the Prandtl number. Given that the total enthalpy is the result of the acoustic power and heat generated in the system, equation 2 is written such as:

$$\dot{H}_{2n}(x) = \dot{E}_{2n}(x) + \dot{Q}_{cn}(x) \quad (3)$$

The coefficient of performance (COP) can be obtained as follows:

$$COP = \frac{\dot{H}_{2n} - \dot{E}_{2n}}{\dot{E}_{2n}} = \frac{\dot{Q}_{cn}}{\dot{E}_{2n}} \quad (4)$$

3.3. Materials selection

3.3.1. Resonator

To select the resonator material, three distinct materials were assessed, as shown in Table 3. The material must possess high thermal resistance to prevent melting at elevated temperatures (400℃) and exhibit low thermal conductivity to minimize heat dissipation. Additionally, the material should demonstrate adequate mechanical strength to withstand operational pressures. The resonator must also be capable of withstanding internal pressures, such as:

$$\sigma_r = p\frac{R}{t} \le \sigma_s = \frac{\sigma_m}{CS} \quad (5)$$

Given p as the internal mean pressure, R as the inner radius of the resonator and t as its thickness, the radial stress σ_r must be less than the maximum allowable stress σ_s, where CS represents the safety factor and σ_m denotes the material's stress. Based on their properties, stainless steel was selected for the study. In the case of stainless steel $\sigma_m = 500\,MPa$, and a safety coefficient $CS = 5$ was set. Thus, Equation 5 yields:

$$\sigma_r = p\frac{R}{t} \le 100\,MPa \quad (6)$$

Analysis revealed that the constraint (σ_r) was satisfied with a maximum resonator thickness (t) of $10\,mm$ and diameters $D_1 = 0.16\,m$ and $D_2 = 0.11\,m$, yielding respectively $32\,MPa$ and $22\,MPa$, which are less than the allowable $100\,MPa$ constraint as detailed in Equation 6.

Table 2. Design parameters

Geometrical parameters	Material parameters	Design parameters
Stack length L_s	Working Fluid	Cooling power Q_c
Central stack position x_c	Thermal conductivity K	Temperature gradient ΔT
Stack space 2l	Speed of sound a	Mean temperature T_m
	Dynamic viscosity ν	Mean pressure p_m
	Isobaric & isochoric compression ratio γ	Pressure amplitude p_1
	Thermal dilatation coefficient β	Frequency f
	Stack material	
	Mean density ρ_s	
	Specific heat c_s	
	Thermal conductivity K_s	

Table 3. Selection of the resonator materials

Materials	**Melting point** (℃)	**Thermal conductivity** (W/mK)	**Mechanical resistance** (N/mm^2)
Mild steel	1370	42.7	485-500
Stainless steel	1400	15	500
Aluminum	660	237	240-300

Table 4. Stack materials

Stack	Description	Value
Honeycomb ceramic	Melting temperature [℃]	1600
	Porosity [CPSI]	230 & 300
	Density $[kg/m^3]$	2500
	Thermal conductivity $[W/mK]$	0.42
	Specific heat $[J/kgK]$	1047
	Melting point [℃]	1450
	Thermal expansion coefficient [℃]	0.7

Table 5. Normalized parameters

Geometrical parameters	Material parameters	Design parameters
Normalized stack length L_{sn} $L_{sn} = \zeta = \frac{2\pi\Delta x}{\lambda} = \frac{2\pi f \Delta x}{a}$	Working Fluid Prandtl number $\sigma = \frac{\mu c_p}{k}$ $\sigma \ll 1$	Normalized cooling power $\dot{Q}_{cn}$ $\dot{Q}_{cn} = \frac{\dot{Q}_c}{Ap_m a} = \frac{\lvert\dot{H}_2\rvert - \lvert\dot{E}_2\rvert}{Ap_m a}$
Normalized central stack position x_c $x_{cn} = \zeta_c = \frac{2\pi}{\lambda}x_c = \frac{2\pi f}{a}x_c$ $0 < x_{cn} < 0.78$	Polytropic coefficient γ $\gamma = 1.667$	Normalized temperature gradient θ $\theta = \Delta T_m = \frac{\Delta T_m}{T_m} = \frac{T_h - T_c}{T_m}$
Normalized thermal penetration depth δ_{kn}	Stack material Specific heat c_s	Drive ratio D $D = \frac{\lvert p_1\rvert}{p_m} = \frac{P_A}{p_m}$
$\delta_{kn} = \frac{\delta_k}{y_0}$ $0.25 < \delta_{kn} < 0.5$ Stack cross-section A Blockage ration B $B = \frac{y_0}{y_0 + l}$ $B \approx 0.8$	Correction factor ϵ_s $\epsilon_s = \sqrt{\frac{\rho_m c_p k}{\rho_s c_s k_s}}$ $\epsilon_s \ll 1$	Mean pressure p_m

3.3.2. Stack

Based on the geometric specifications of the stack as a function of the COP, it has been found that configurations incorporating stacks within a network of pins, followed by those with parallel plates, exhibit the highest efficiency. Although Mylar is commonly used as a stack material, its melting point is limited to 232℃. Consequently, honeycomb stacks have been selected due to their ability to withstand temperatures up to 1450℃ [21]. The properties of honeycomb ceramics are detailed in Table 4.

3.3.3. Working fluid

The selection of the working fluid was evaluated based on the Prandtl number, defined as follows:

$$\sigma = \left(\frac{\delta_v}{\delta_k}\right)^2 \tag{7}$$

With δ_k and δ_v respectively, the thermal and viscous penetration depths. A low Prandtl number reduces both viscous and thermal losses. Therefore, the working fluid should possess a low melting point, high sound speed, and inertness to the components of the refrigeration system [8]. Helium was selected as the working fluid due to its favorable properties, including a low Prandtl number of 0.72 at 20℃.

3.3.4. Mean Pressure

From Equation 8, the acoustic power is dependent on the pressure within the system. The latter is determined by solving the Rott wave differential equation (Equation 9).

$$\frac{d\dot{E}}{dx} = -\frac{r_v}{2}|U_1|^2 - \frac{1}{2r_k}|p_1|^2 + \frac{1}{2}Re[g\tilde{p}_1 U_1] \tag{8}$$

$$[1+(\gamma-1)f_k]p_1 + \frac{\gamma p_m}{\omega^2}\frac{d}{dx}\left(\frac{1-f_v}{\rho_m}\frac{dp_1}{dx}\right) - \frac{a^2}{\omega^2}\frac{f_k - f_v}{1-\sigma}\frac{1}{T_m}\frac{dT_m}{dx}\frac{dp_1}{dx} = 0 \tag{9}$$

With r_v the hydraulic radius, U_1 the volume flow rate, p_1 the pressure, which is complex and $\tilde{p}_1$ his conjugate, g the complex gain force, f_k and f_v spatial averages of complex function which depends on the specific channel geometry under consideration, p_m the mean pressure, ρ_m the mean density and ω the angular velocity. Assuming the constant variation in mean temperature dT_m / dx is known, solving Equation 9 yields the mean pressure $|p_1|$. This pressure serves as the upper limit for resonator material selection. For this study, an average pressure of 20 bar is adopted.

3.3.5. Frequency

To enhance stack performance, the resonance frequency of the system must align with the acoustic resonance frequency of the gas. This frequency is computed as:

$$f = \frac{a}{\lambda} \tag{10}$$

Table 6. Global parameters

Operating Parameters	Concept 1	Concept 2
Mean pressure p_m [bar]	20	20
Mean temperature T_m [K]	657.16	657.49
Frequency f [Hz]	170.73	441.28
Pressure amplitude $\|p_1\|$ or P_A [bar]	1.388	1.087

Enhancing performance through resonator length, a resonator with a length $L = \lambda/4$ to amplify the temperature difference within the stack has been selected, which enables the achievement of optimal performance. Consequently, Equation 10 is equivalent to

$$f = \frac{a}{4L} \tag{11}$$

4. TADTAR Geometrical Configuration

4.1. Configuration Selection

Through DeltaEC analysis, global parameters for standing and traveling wave configurations were calculated at a maximum residual heat input of 10 kW. As shown in Table 6, the standing wave configuration achieved a mean pressure of 20 bar, temperature of 657.16 K, and frequency of 170.73 Hz, while the traveling wave configuration reached 20 bar, 657.49 K, and a higher frequency of 441.28 Hz. The frequency is influenced by heat input and geometric configuration. While higher frequency benefits TAE, it can induce dissipation in TAR, leading to similar behavior in TADTAR.

Thus, as shown in Figure 7, results indicate a maximum COP of 0.4 for the traveling wave system at a 9 kW residual heat load (Concept 2), compared to 1.5 for the standing wave system at a 10 kW heat load (Concept 1). Given the heat input, the selected geometrical parameters yielded a COP that aligns with literature values. However, the COP remains lower than that of traditional systems. Based on these preliminary results, the standing wave configuration was chosen for further numerical analysis in DeltaEC to investigate the TADTAR's performance. Based on the developed geometry, a 3D model was created using SolidWorks (Figure 8). Practically, the hot exchanger (HHX) is connected to the exhaust engine pipe, the first ambient heat exchanger (AHX1) to an ambient temperature water source, the second ambient heat exchanger (AHX2) to a second water source, and the cold heat exchanger (CHX) to the vehicle cabin.

4.2. Length of the Stack

To assess the thermoacoustic refrigerator's performance, four stacks with lengths (L_s) of 0.4, 0.3, 0.2, and 0.1 meters were employed. Each stack was sequentially tested on both the TAE and TAR regions while maintaining constant dimensions for all other components. Figure 9 depicts the stack length arrangement on the TADTAR.

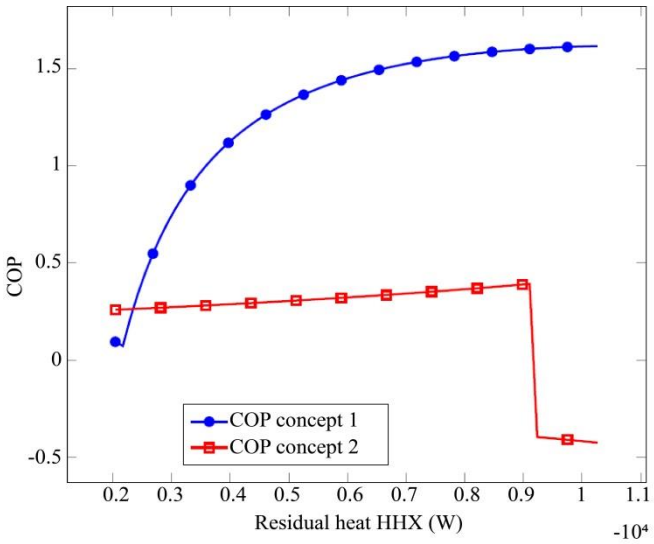

Fig. 7 Evaluation of COPs of standing and traveling wave

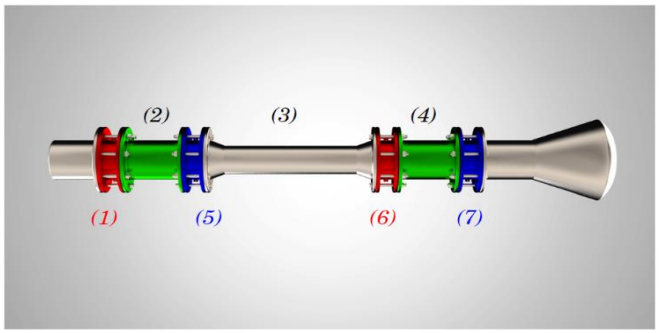

Fig. 8 3D model of the TADTAR composed with the following: (1) HHX, (2) TAR STACK, (3) RESONATOR, (4) TAE STACK, (5) AHX1, (6) AHX2, (7) CHX.

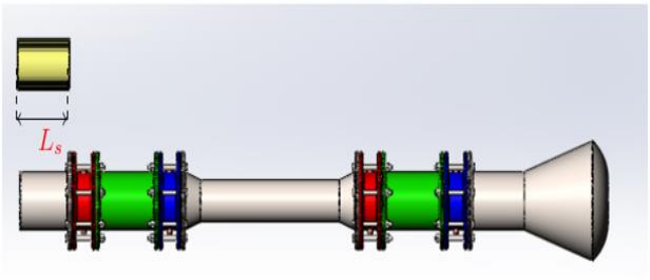

Fig. 9 Stack length

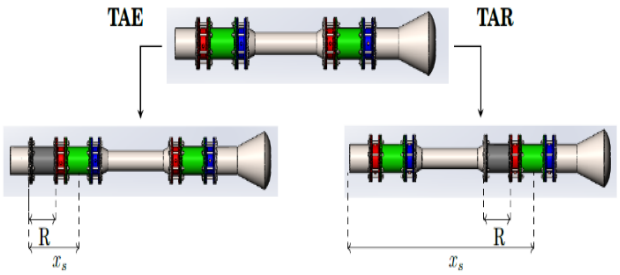

Fig. 10 Stack position on the TAE and TAR sides

Table 7. Stack positioning measurement

Component R (m)	Position x_s on TAE (m)	Position x_s on TAR (m)
0	0.35	1.27
0.1	0.45	1.37
0.25	0.6	1.52
0.35	0.7	1.62
0.45	0.8	1.72

4.3. Position of the Stack

To modify the TAE and TAR stack positions (x_s), an extension component (R) of varying size, as detailed in Table 7, was introduced. Figure 10 depicts the integration of component R into the resonator on both the engine and refrigerator sides, consequently adjusting the stack placement relative to the pressure antinode. Table 7 outlines the values assigned to R and the resulting TAE and TAR stack positions.

4.4. Space Between Plates

Given the requirement for imperfect thermal contact between the stack and oscillating gas in standing wave refrigerators [11], plate spacing ($2y_0$) was varied within the range of $2\delta_k \leq 2y_0 \leq 4\delta_k$ to evaluate system performance, with $\delta_k = 0.45 \times 10^{-4}\ m$.

4.5. Plate Thickness

The influence of plate thickness on thermoacoustic refrigerator performance was investigated while maintaining constant dimensions for other components. Initially, the impact of TAE stack plate thickness is assessed with TAR stack plate thickness held constant. Subsequently, the effect of TAR stack plate thickness is evaluated with the TAE stack thickness fixed. Thickness values ranging from 1 to 10 mm have been considered for both analyses.

5. Numerical Analysis and Discussion

5.1. Temperature and Pressure Distribution

Figure 11 (a) provides evidence of the gas temperature variation along the resonator, exhibiting in the TAE's stack region (between HHX and AHX1), a hot heat exchanger operating at a temperature of $673\ K$, when subjected to a $13\ kW$ heat load. Heat transfer to the gas results in a mean gas temperature of $657{,}16\ K$. This satisfies the condition. $T_m > \Delta T_{m,E} = 391.09K$ for a TAE, where the mean temperature must exceed the temperature difference between the stack ends to bear a thermoacoustic engine characteristic. In the TAR's stack region (between AHX2 and CHX), the system absorbs heat with $T_m < \Delta T_{m,C} = 67{,}34\ K$. This confirms adherence to the critical temperature condition to bear a thermoacoustic refrigerator characteristic [10]. As described in Figure 11 (b), the selected configuration exhibits a maximum pressure of $1.4 \times 10^5\ Pa$ at the system inlet at position $x = 0\ m$, corresponding to the pressure antinode. With the selected resonator length approximating a quarter wavelength, a pressure node is established at position $x = 1,2\ m$.

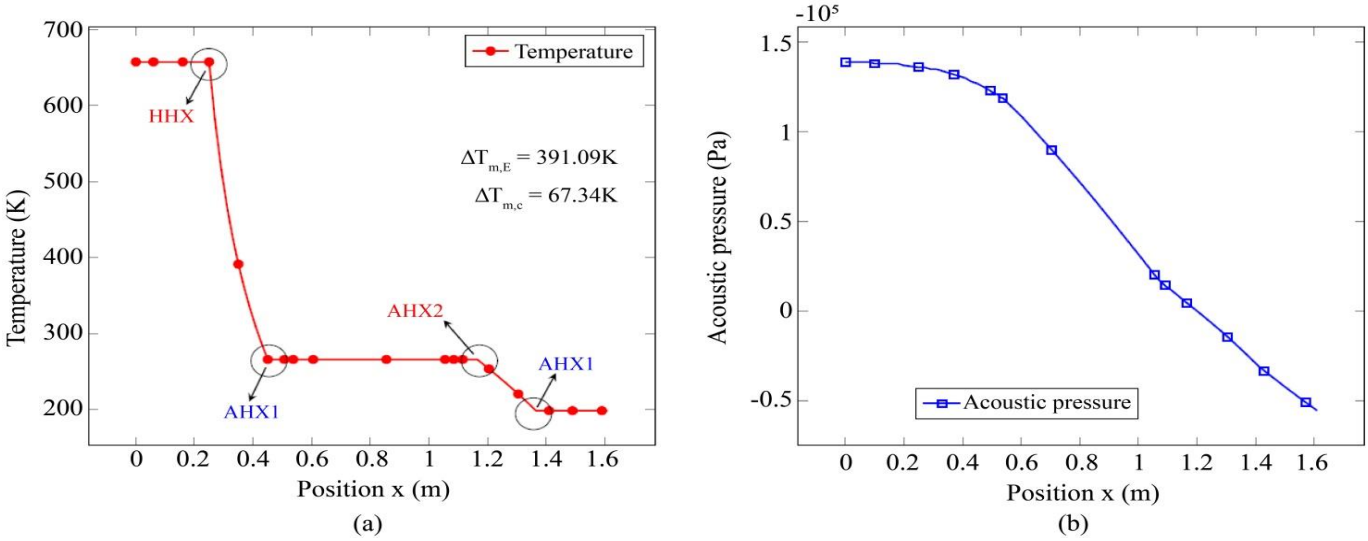

Fig. 11 Temperature (a) and pressure (b) distributions in the system.

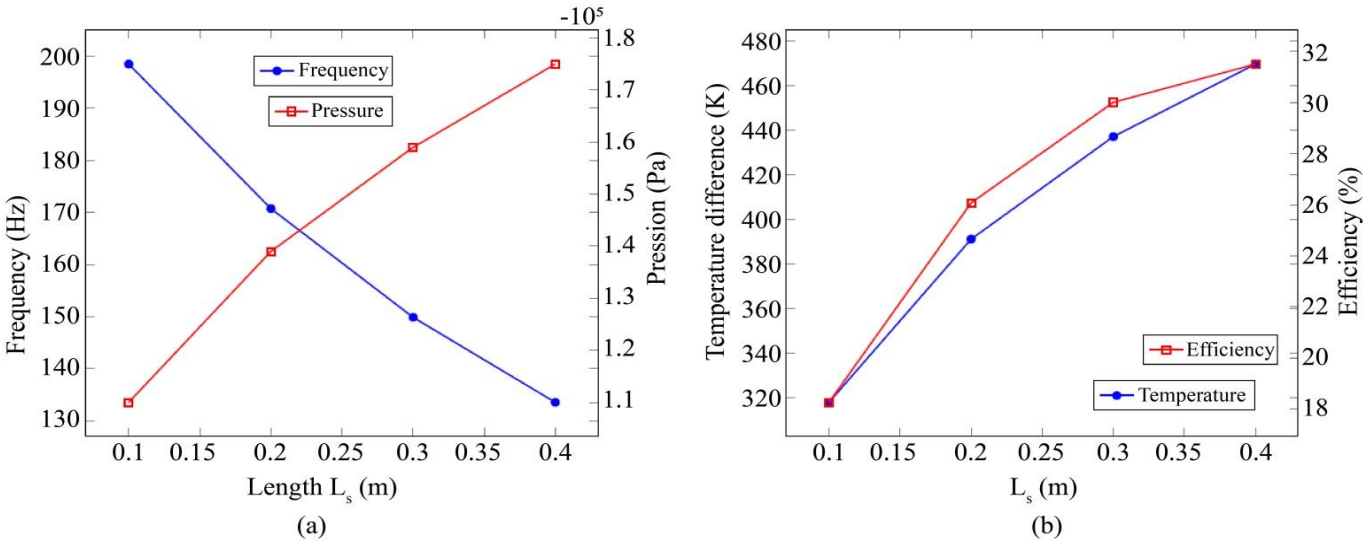

Fig. 12 TAE stack length analysis: Evaluation of (a) Frequency and pressure (b) Temperature difference and Efficiency.

Hence, placing the TAE and TAR stacks respectively at pressure antinode and node leads to greater performance of the TADTAR. This is because, in a standing wave thermoacoustic system, the acoustic power is proportional to pressure. Conversely, the cooling power is high for low-pressure generations, specifically at nodal points.

5.2. Stack Length Analysis

In the TAE region, stack lengths of 0.1,0.2, 0.3 and 0.4 m reached a pressure of $1.1 \times 10^5, 1.4 \times 10^5, 1.6 \times 10^5$ and $1.78 \times 10^5\ Pa$, respectively. As the engine stack was systematically placed near the pressure antinode, this result indicated that the sound pressure rises proportionally with TAE stack length. Conversely, the resonant frequency decreased inversely with stack length, resulting in maximum pressure at lower angular frequencies for the longest stack. Thus, the highest frequency was reported for a stack length of $0.1\ m$. The pressure and frequency analyses on the TAE stack are depicted in Figure 12 (a). In addition, it was found, as indicated in Figure 12 (b), that the temperature difference is proportional to the stack length, reporting a maximum temperature of 460℃ for the stack length of $0.4\ m$.

This result confirmed the intricate relationship between pressure and temperature in the thermoacoustic system, where a pressure variation leads to temperature variation and vice versa. Besides, Figure 12 (b) revealed that the efficiency of the TAE is high for the longest stack length. The efficiency subsequently improved with rising temperatures as stack length increased, reaching 32% for a stack length of $0.4\ m$. In the TAE region, the increase in temperature and pressure with the stack length might be due to the necessity to have a higher input power to overcome the viscous losses proportional to the resonator length, as reported by Balonji et al. [23].

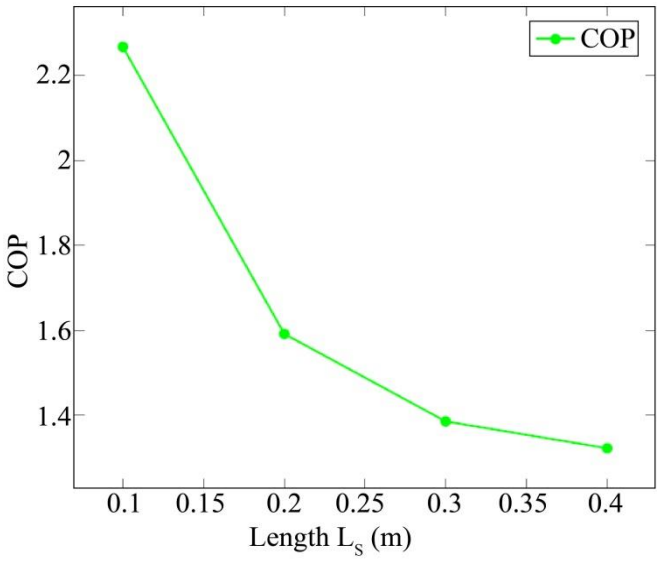

Fig. 13 COP as a function of the regenerator length

However, Figure 13 revealed that the COP of the TADTAR tends to decline with a larger TAE stack due to increased acoustic power dissipation within the resonator and heat exchangers. The system reached the lowest and highest COP of 1.2 and 2.3 for a stack length of 0.4 m and 0.1 m, respectively.

These findings indicate that while greater acoustic power is generated with a longer TAE stack, it does not necessarily translate to enhanced heat transfer in the refrigerator region. Consequently, a smaller TAE stack is recommended for better TADTAR performance. In the TAR region, stack lengths of 0.1,0.2, 0.3 and 0.4 m, reached a pressure of $1.43 \times 10^5, 1.4 \times 10^5, 1.37 \times 10^5$ and 1.35×10^5 Pa, respectively. This result indicated the pressure drop with a longer TAR stack. By lengthening the stack, its position shifted near the pressure node and led to imperfect thermoacoustic exchanges.

This result was corroborated by frequency and temperature drops in the TAR region, as shown in Figure 14 (a), leading to low COP, as depicted in Figure 14 (b). This might also be explained by the fact that effective heat exchange between the stack and gas, transforming acoustic work into heat, hinges on a stack with a length smaller than half of the acoustic wavelength [11]. Therefore, a shorter TAR stack positioned nearer to the pressure node is recommended for a TADTAR, as it exhibits superior performance, minimizing acoustic power while maximizing cooling power.

5.3. Stack Position Analysis

In the TAE region, with the stack positioned respectively at 0.35, 0.45, 0.6 and 0.7 m, as depicted in Table 7, ia decrease in the frequency, pressure, temperature difference and efficiency of the engine was observed. This result, depicted in Figure 15 (a), exhibits the inverse relationship between the TAE stack position and both resonance frequency and acoustic pressure in the TADTAR.

This correlation leads to reduced stack temperature difference and overall system efficiency, as shown in Figure 15 (b). Consequently, TAE performance diminishes when the stack is positioned farther from the pressure antinode. Conversely, Figure 16 indicated the highest COP of 4 for the stack positioned at 0.9 m. This result revealed that the COP of the TADTAR is high for a TAE stack positioned farther from the acoustic antinode, leading to a relatively low frequency and pressure and maximizing the cooling capacity.

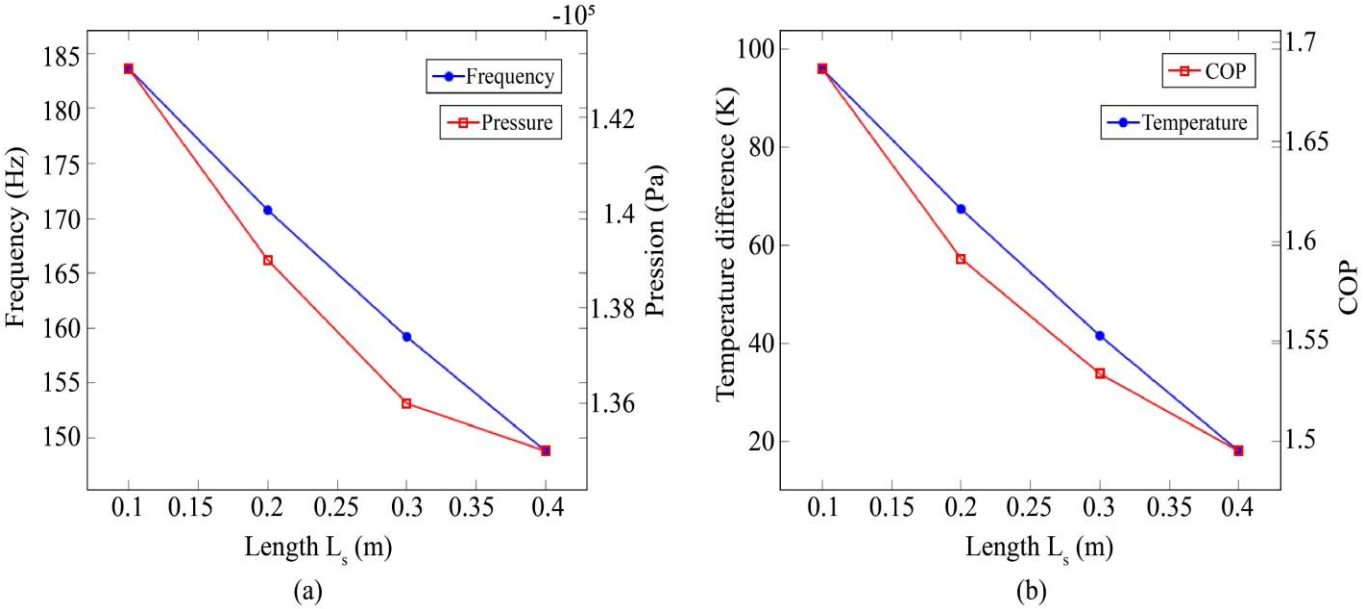

Fig. 14 TAR stack length analysis: Evaluation of (a) Frequency and pressure (b) Temperature difference and C.

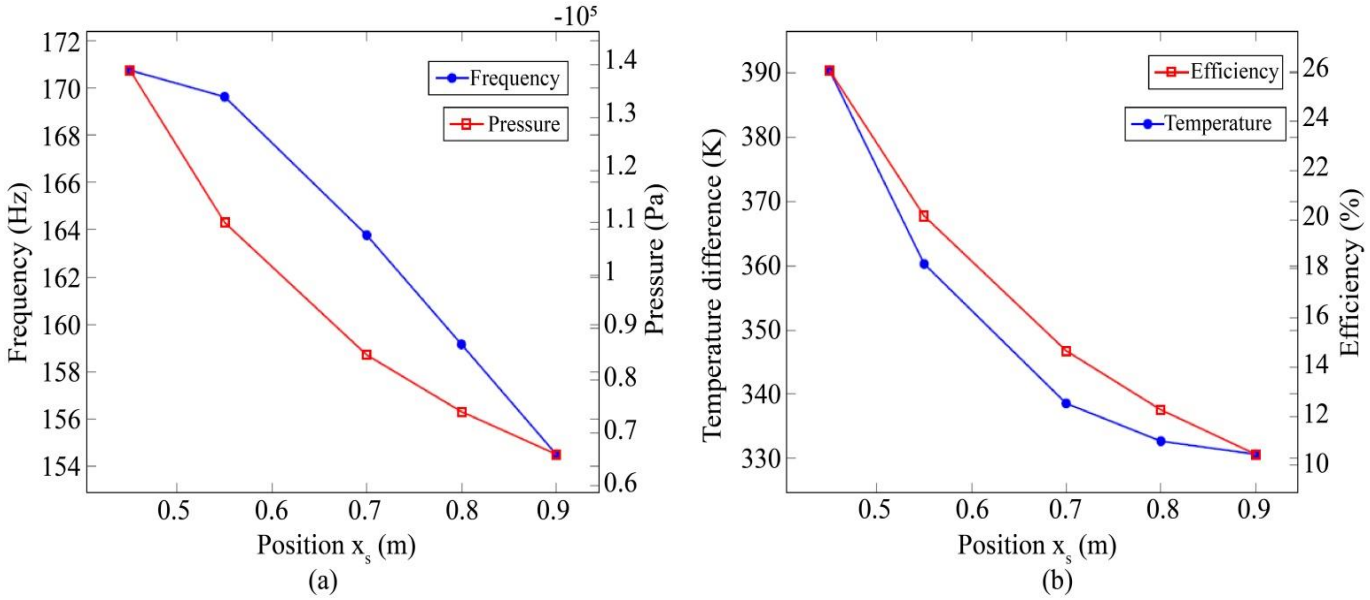

Fig. 15 TAE stack position analysis: Evaluation of (a) Frequency and Pressure (b) Temperature difference and Efficiency.

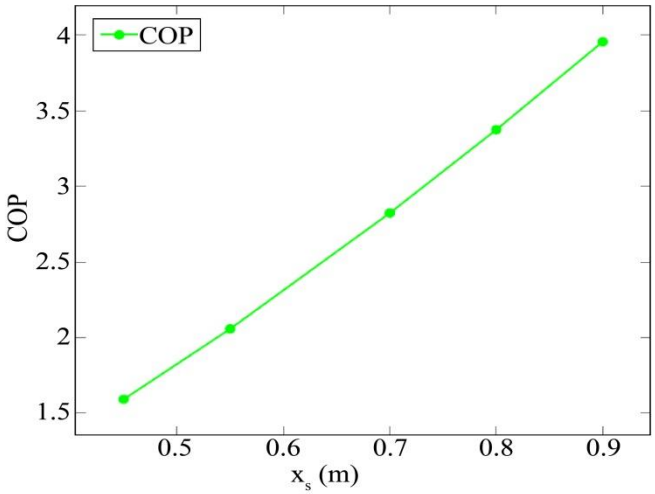

Fig. 16 COP as a function of the regenerator position

In Figure 17 (a), an inverse relationship between the frequency and the pressure in the TAR region was observed as the stack was positioned farther from the pressure node. The frequency and pressure attained, respectively 1.46×10^5 Pa and $145\ Hz$ for a maximum stack position at $1.72\ m$. Unlike the TAE region, where positioning negatively impacts pressure but leads to great COP, positioning the TAR stack slightly away from the pressure node reduces performance in the TAR region. Therefore, as depicted in Figure 17 (b), the maximum COP of 4 was attained for the initial TAR stack at $1.27\ m$, given in Table 7. Consequently, suitable TADTAR performance is achieved by positioning the TAR stack close to the pressure node.

5.4. Spacing of TAE and TAR Plates

The spacing of the TAE and TAR stack plates was investigated within the range of $2\delta_k \leq 2y_0 \leq 4\delta_k$ with $\delta_k = 0.45 \times 10^{-4}\ m$. The analysis in Figure 18 (a) revealed that increasing the space between the TAE stack plates leads to high-frequency generation and, subsequently, a low COP. This result indicated that managing high frequencies in the TADTAR system can lead to acoustic power and heat losses as we tend to increase the space between the plates and enhance the performance.

Therefore, the imperfect thermal contact between plates in the TAE region introduces thermal resistance, dissipating acoustic energy as heat. Conversely, a similar plate spacing on the TAR stack side yields a high frequency and COP, signifying greater performance and reduced energy consumption within the stack.

As presented in Figure 18 (b), the highest COP of 1.56 was obtained for a spacing between the plates of $1.8 \times 10^{-4}\ m$ corresponding to $4\delta_k$. This might be explained by the fact that effective heat exchange between the stack and gas in the TAR region, transforming acoustic work into heat, hinges on imperfect thermal contact. This condition is characterized by thermal penetration depth (δ_k) and viscous penetration depth (δ_v) being smaller than the stack's wavelength (λ). Practically, imperfect thermal contact might dampen plate vibrations, mitigating instability and temperature fluctuations.

5.5. Thickness of TAE and TAR Plates

Figure 19 revealed that the COP on both the engine and refrigerator analyses remain constant at a value of 1.6. This result indicates that plate thickness exerts minimal influence on overall system performance. This is due to the selection of plate thickness within an acceptable range, which ensures adequate thermal contact between plates and gas. Thus, for the TADTAR analysis, with a plate thickness between 0.1 and $1\ mm$, the system's COP remains unaffected.

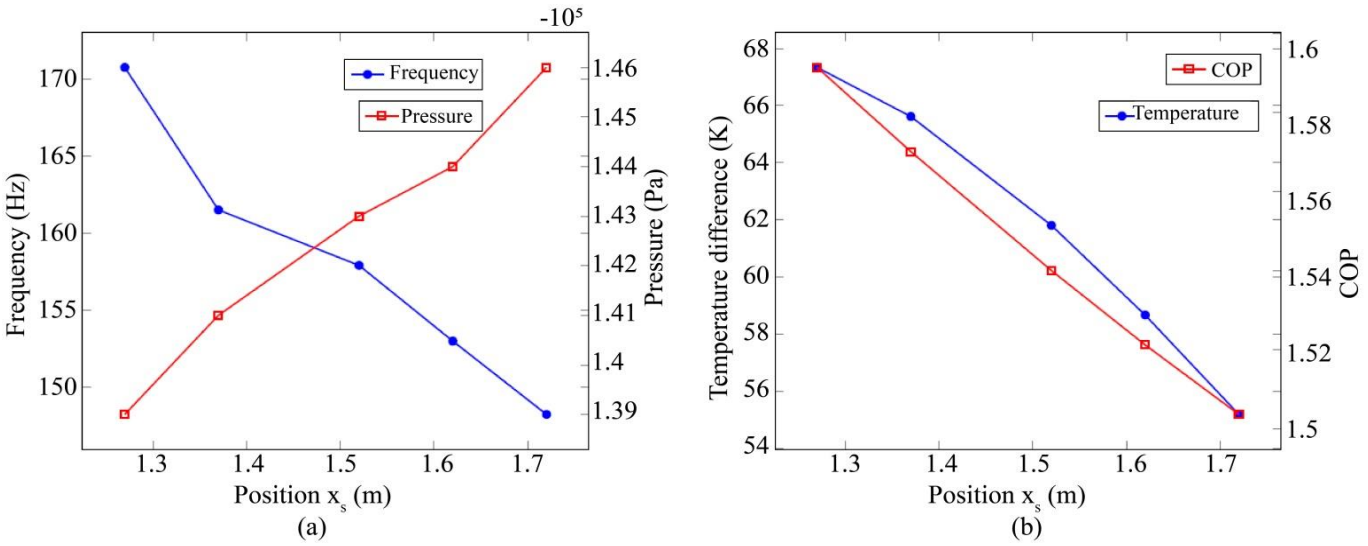

Fig. 17 TAR stack position analysis: Evaluation (a) Frequency and pressure (b) Temperature and COP.

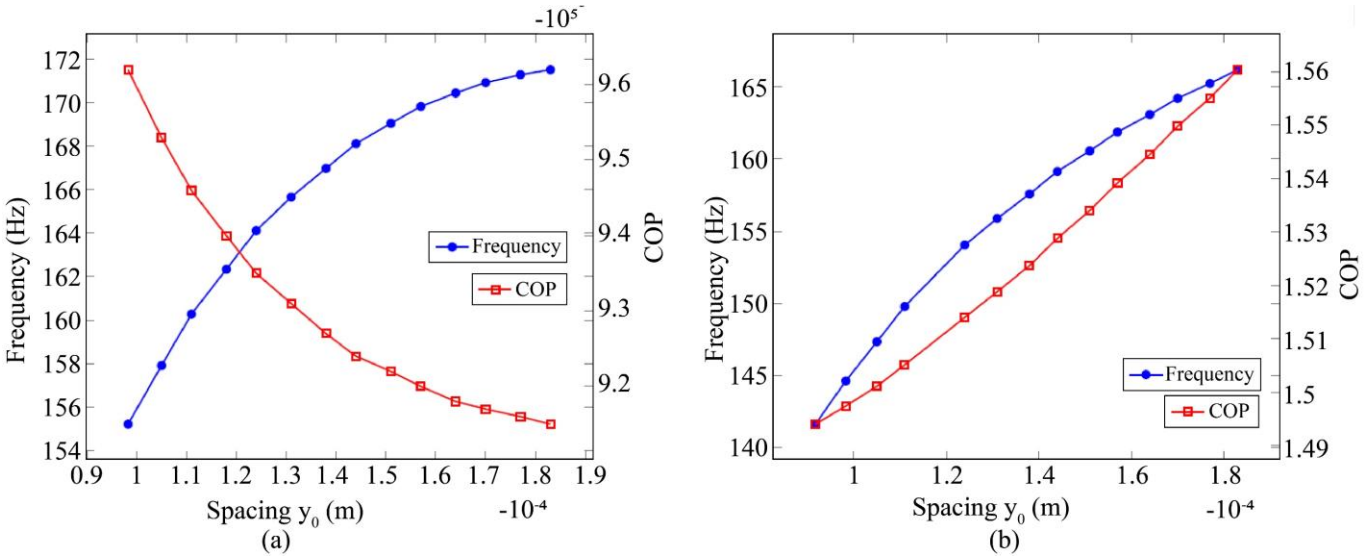

Fig. 18 Stack plate spacing evaluation of the frequency and COP for: (a) TAE stack (b) TAR stack.

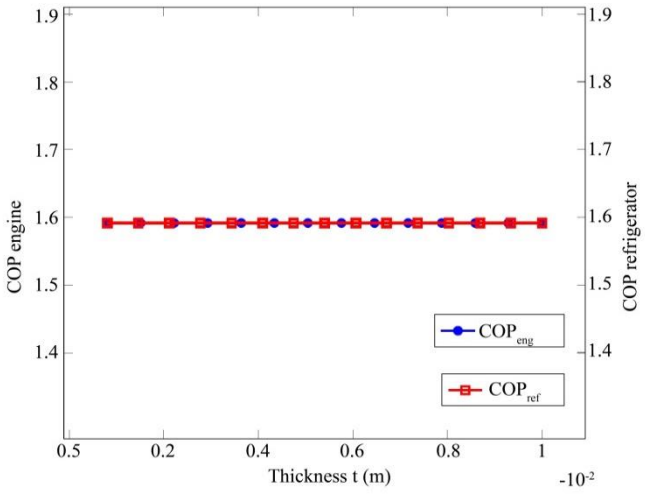

Fig. 19 Plate thickness analysis on system performance

Table 8. Geometrical parameters for maximum performance

	Length (m)	Position (m)	Spacing (m)	Thickness (m)
TAE stack	0.1	0.5	0.0001	0.005
TAR stack	0.1	1.3	0.0018	0.005

5.6. Performance Settings

Based on the preceding analysis, enhancing heat transfer within the thermoacoustic refrigerator necessitates a short TAE stack positioned away from the pressure antinode coupled with a compact TAR stack situated near the pressure node. Therefore, the best design parameters leading to high COP in each of the analyses conducted were selected to model the enhanced TADTAR, as presented in Figure 20. The detailed geometrical parameters of this configuration are presented in Table 8 and serve as a foundation for subsequent modelling in DeltaEC.

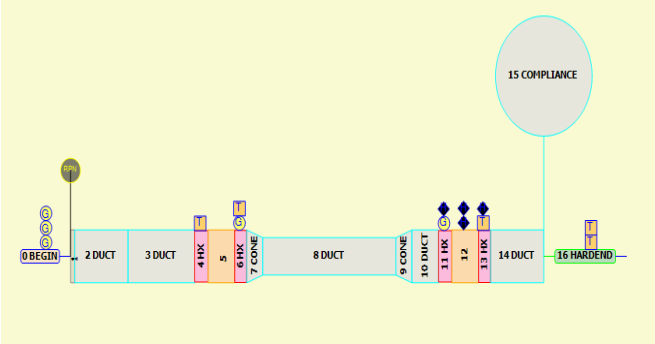

Fig. 20 Final TADTAR configuration

Depending on the quantity of heat (Q_h) at the entrance to the hot heat exchanger, as well as the quantity of heat (Q_c) to be supplied to the cold exchanger to cool the cabin, the overall COP was computed and varied, as shown in Figure 21. Thus, considering the study of a heavy vehicle as specified in the requirements, suitable performances of the TADTAR system were found and tabulated in Table 9. The TADTAR achieved a maximum COP of 4 for a cold thermal power of 5372 W, a resonance frequency of 170.68 Hz, and a cooling temperature of 200 K. This analysis resulted in a substantial enhancement of the coefficient of performance, surpassing the preliminary value of 1.5. This translates to a COP relative to Carnot efficiency of 73.09%, indicating a significant improvement in the system's thermodynamic performance. However, in an experimental case, the system performance could be lower due to leaks, heat dissipation and construction defects. It is thus crucial to validate these results through experimental tests.

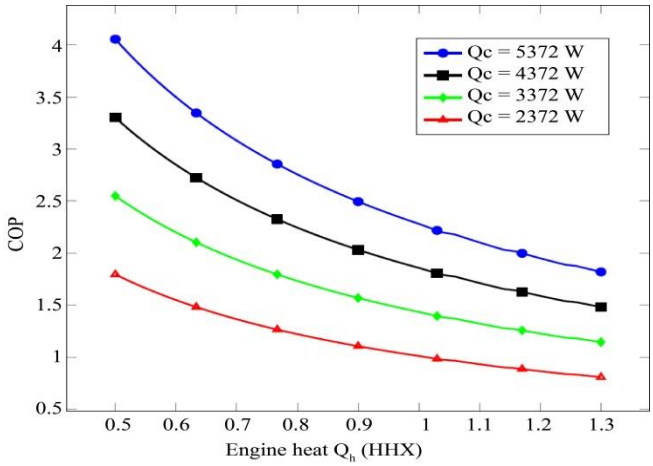

Fig. 21 Overall COP of the TADTAR

Table 9. TADTAR performance

Parameters	Values
Frequency	170.68 Hz
Pressure	1.22×10^5 Pa
COP	4
COP/COP*carnot*	73.09%
Minimum temperature	200 K

6. Conclusion

This article presents the design and analysis of a thermoacoustic refrigerator with a thermoacoustic drive (TADTAR) powered by residual heat. The TADTAR system exploits the thermoacoustic effect to convert waste heat into acoustic energy, which is then used to pump heat from a cold source to a hot source. The sizing of the TADTAR was carried out using DeltaEC software, which allows for the simulation of design performance. The simulation results showed that the length and position of the TAE and TAR stacks, as well as the spacing and thickness of the plates, significantly impact the system's performance. The enhanced TADTAR configuration has a TAE stack length of 0.1 m, a position of 0.5 m, a plate spacing of 0.0001 m, a TAR stack length of 0.1 m, a position of 1.3 m, a plate spacing of 0.0018 m, and a plate thickness of 0.005 m. This configuration achieved a maximum coefficient of performance (COP) of 4 for a cold thermal power of 5372 W, a resonance frequency of 170.68 Hz, and a cooling temperature of 200 K. The results of this study demonstrate the feasibility of designing a TADTAR powered by the waste heat from heavy vehicle exhaust gases. The system shows promising performance and could be used to reduce vehicle energy consumption and emissions.

Abbreviation	
AHX	Ambient Heat Exchanger
CHX	Cold Heat exchanger
CFC	Chlorofluorocarbon
COP	Coefficient Of Performance
HDTAR	Heat Driven Thermoacoustic Refrigerator
HFC	Hydrofluorocarbon
HHX	Hot Heat Exchanger
MP	Material Parameter
TADTAR	Thermoacoustically-Driven Thermoacoustic Refrigerator
TAE	Thermoacoustic Engine
TAR	Thermoacoustic Refrigerator
RPN	Reverse Polish Notation

References

[1] Mohanad Q. Kamil, Samir Gh. Yahya, and Itimad D.J. Azzawi, "Design Methodology of Standing-Wave Thermoacoustic Refrigerator: Theoretical Analysis," *International Journal of Air-Conditioning and Refrigeration*, vol. 31, pp. 1-13, 2023. [CrossRef] [Google Scholar] [Publisher Link]

[2] Luke Zoontjens et al., "Feasibility Study of an Automotive Thermoacoustic Refrigerator," *In Proceedings of Acoustics*, Busselton, Australia, pp. 363-371, 2005. [Google Scholar] [Publisher Link]

[3] Stijn Broekaert et al., "Assessment of Waste Heat Recovery for Heavy-Duty Vehicles during On-Road Operation," *Applied Thermal Engineering*, vol. 5, 2021. [CrossRef] [Google Scholar] [Publisher Link]

[4] Vipin Nair, "HFO Refrigerants: A Review of Present Status and Future Prospects," *International Journal of Refrigeration*, vol. 122, pp. 156-170, 2021. [CrossRef] [Google Scholar] [Publisher Link]

[5] Anne de Jong, "*Numerical Modeling of Thermoacoustic Systems*," PhD Thesis, University of Twente, 2015. [CrossRef] [Google Scholar] [Publisher Link]

[6] Jay A. Adeff, and Thomas J. Hofler, "Design and Construction of a Solar-Powered, Thermoacoustically Driven, Thermoacoustic Refrigerator," *Journal of Acoustical Society of America*, vol. 107, pp. L37-L42, 2000. [CrossRef] [Google Scholar] [Publisher Link]

[7] M.E.H. Tijani, J.C.H. Zeegers, and A.T.A.M. De Waele, "Design of Thermoacoustic Refrigerators," *Cryogenics*, vol. 42, no. 1, pp. 49-57, 2002. [CrossRef] [Google Scholar] [Publisher Link]

[8] Gregory W. Swift, and Steven L. Garrett, "Thermoacoustics: A Unifying Perspective for Some Engines and Refrigerators," *Journal of the Acoustical Society of America*, vol. 113, pp. 2379-2381, 2003. [CrossRef] [Google Scholar] [Publisher Link]

[9] T. Yazaki et al., "Traveling-Wave Thermoacoustic Engine in A Looped Tube," *Physical Review Letters*, vol. 81, pp. 3128-3131, 1998. [CrossRef] [Google Scholar] [Publisher Link]

[10] S. Backhaus, and Gregory W. Swift, "A Thermoacoustic-Stirling Heat Engine: Detailed Study," *The Journal of the Acoustical Society of America*, vol. 107, pp. 3148-3166, 2000. [CrossRef] [Google Scholar] [Publisher Link]

[11] Serge Dufourd, "*Thermoacoustic Refrigerator: Analytical and Experimental Studies for Miniaturization*," Doctoral Thesis, Ecole Centrale de Lyon, 2001. [Google Scholar]

[12] Ram C. Dhuley, and M. D. Atrey, "Design Guidelines for a Thermoacoustic Refrigerator," *Arxiv*, pp. 1-6, 2016. [CrossRef] [Google Scholar] [Publisher Link]

[13] M.E.H. Tijani, "*Loudspeaker-Driven Thermo-Acoustic Refrigeration*," Phd Thesis, Applied Physics and Science Education, 2001. [CrossRef] [Google Scholar] [Publisher Link]

[14] B.G. Prashantha et al., "Effect of Gas Spacing and Resonance Frequency on Theoretical Performance of Thermoacoustic Refrigerators," *International Journal of Air-Conditioning and Refrigeration*, vol. 31, pp. 1-14, 2023. [CrossRef] [Google Scholar] [Publisher Link]

[15] Sophie Cordillet, "Modeling and Dimensioning of a Solar Receiver for A Thermoacoustic Cold Production System," Doctoral Dissertation, Université Paris Sud-Paris, pp. 1-206, 2013. [Google Scholar]

[16] Simon Spoelstra, "*ThermoAcoustic Technology for Energy Applications*," Final Report, pp. 1-48, 2012. [Publisher Link]

[17] Patcharin Saechan, and Isares Dhuchakallaya, "Design and Experimental Evaluation of a Travelling Wave Thermoacoustic Engine," *Energy Reports*, vol. 6, no. S9, pp. 1456-1461, 2020. [CrossRef] [Google Scholar] [Publisher Link]

[18] Irna Farikhah, "*Optimization of A Heat Driven Thermoacoustic Cooler in A Looped Tube with Two Stacks*," Doctoral Thesis, Tokyo University of Agriculture and Technology, 2018. [Google Scholar] [Publisher Link]

[19] Zahra Bouramdane et al., "Numerical Analysis of Thermoacoustically Driven Thermoacoustic Refrigerator with A Stack of Parallel Plates Having Corrugated Surfaces," *International Journal of Air-Conditioning and Refrigeration*, vol. 30, pp. 1-19, 2022. [CrossRef] [Google Scholar] [Publisher Link]

[20] A.B. Desai et al., "Experimental Study and Analysis of a Thermoacoustically Driven Thermoacoustic Refrigerator," *Sadhana*, vol. 45, 2020. [CrossRef] [Google Scholar] [Publisher Link]

[21] Martin Wetzel, and Cila Herman, "Design Optimization of Thermoacoustic Refrigerators," *International Journal of Refrigeration*, vol. 20, no. 1, pp. 3-21, 1997. [CrossRef] [Google Scholar] [Publisher Link]

[22] Channarong Wanthaa, and Kriengkrai Assawamartbunluea, "The Impact of The Resonance Tube on Performance of a Thermoacoustic Stack," *Frontiers in Heat and Mass Transfer (FHMT)*, vol. 2, no. 4, pp. 1-8, 2011. [CrossRef] [Google Scholar] [Publisher Link]

[23] S. Balonji et al., "Performance Alteration of Standing-Wave Thermoacoustically-Driven Engine through Resonator Length Adjustment," *Procedia Manufacturing*, vol. 35, pp. 1350-1355, 2019. [CrossRef] [Google Scholar] [Publisher Link]